Supplementary information

Ultrahigh output energy density of explosive-energy-conversion devices assembled by multilayer ferroelectric films

Zhengwei Xiong[1#], Zhangyang Zhou[2#], Yi Liu[3#], Zhengqian Fu[4], Fangfang Xu[4], Leiming Fang[5], Xiaoru Liu[1], Jun Li[3], Ke Jin[3], Zhipeng Gao[1,3]*

1 Joint Laboratory for Extreme Conditions Matter Properties, School of Mathematics and Physics, Southwest University of Science and Technology, Mianyang 621010, China.

2 College of Intelligent Systems Science and Engineering, Hubei Minzu University, Enshi, 445000, China.

3 Institute of Fluid Physics, China Academy of Engineering Physics, Mianyang 621900, China.

4 State Key Laboratory of High Performance Ceramics and Superfine Microstructures, Shanghai Institute of Ceramics, Chinese Academy of Sciences, Shanghai 200050, China.

5 Institute of Nuclear Physics and Chemistry, China Academy of Engineering Physics, Mianyang 621900, China.

[#]Zhengwei Xiong, Zhangyang Zhou and Yi Liu contributed equally to this work.

*Corresponding author E-mail address:

Zhipeng Gao (z.p.gao@foxmail.com)

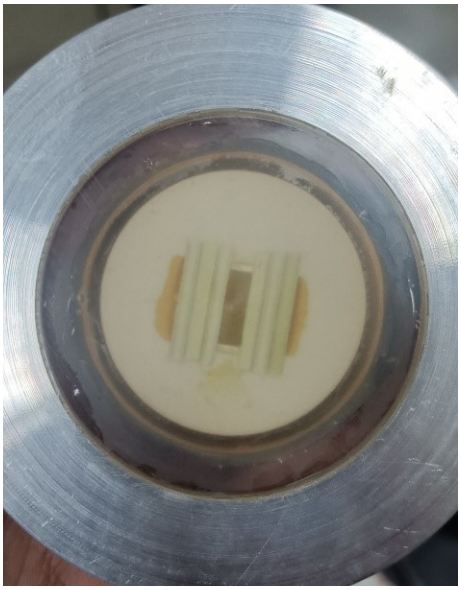

Fig. S1 The diagram of the experimental set-up for multilayer PMN-PZT films.

In the Hugoniot experiment, the PMN-PZT+2Li film was used to impact the LiFe window (Fig. S2), and the particle velocity at the interface in front of the window was measured using a laser interferometer. The Hugoniot curve of the film sample was subsequently determined through the impedance matching method [1, 2].

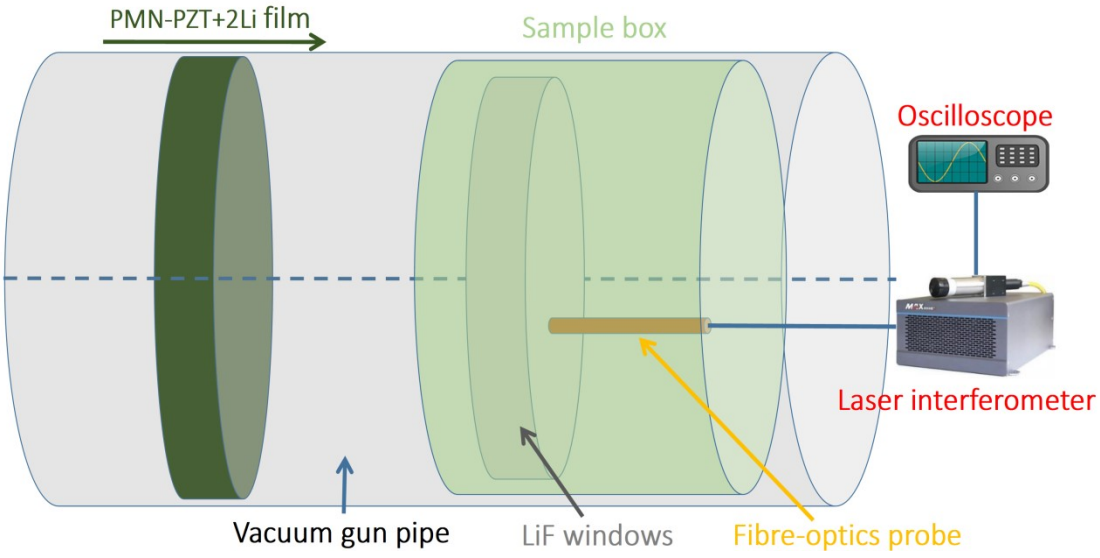

Fig. S2 Schematic diagrams of Hugoniot experiment

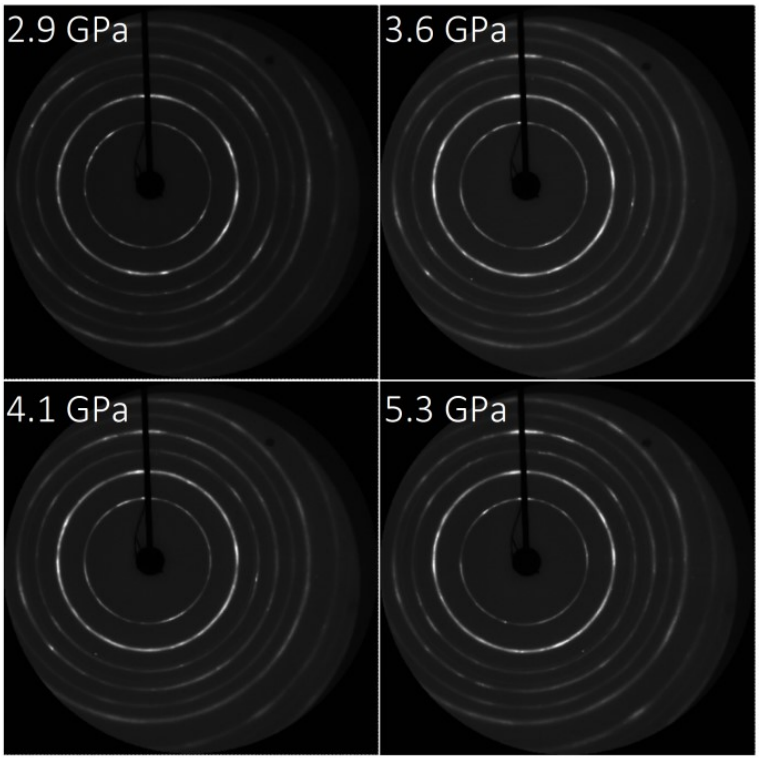

Fig. S3 2D Debye-Scherrer rings for the synchrotron X-ray diffraction patterns of PMN-PZT+2Li crystal at selected pressures with ambient temperature.

Fig. S4 shows the temperature stability of d_{33} for the original, 10 days-aging and 30 days-aging films, respectively. The aging temperature is 80 ℃. After accelerated aging for 30 days, the d_{33} of the film sample is still above 597 pC/N within the temperature range of 5 - 200 ℃. The value is significantly higher than that of the reported ferroelectric material for explosive-energy-conversion ($K_{0.5}Na_{0.5}NbO_3$ and $Na_{0.5}Bi_{0.5}TiO_3$) [3-5], and even surpasses the excellent soft PZT-5H (d_{33} ~ 590 pC/N) [6-9]. The large d_{33} value originates from the abundant nanoscale domain structures within the grains (Fig. 1c) [6-8], suggesting the remarkable advantages of PMN-PZT+2Li films in rapid energy transfer. Furthermore, the room-temperature d_{33} value decreases by only 2.80% from 644 to 626 pC/N after 30-days aging, demonstrating the long-term storage capability of the films.

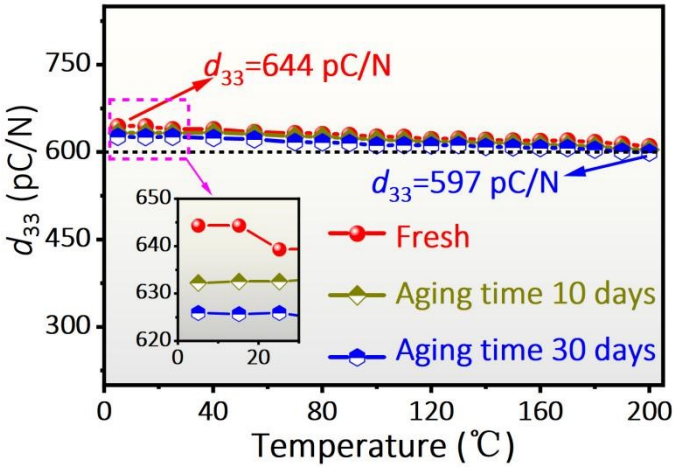

Fig. S4 Temperature stability of d_{33} for PMN-PZT+2Li films.

Fig. S5 illustrates the observed current I and release charge Q in the single-layer PMN-PZT+2Li films under varying shock pressures. At 1.2 GPa (Fig. S5a), a typically small piezoelectric effect current is observed with a small Q (r = 23.65%), and the waveform exhibits vibrating, reaching a maximum positive current of 6.78 A. As the pressure increases to 2.8 GPa (Fig. S5b), a higher maximum positive current of 9.44 A is recorded, while the released charge of 26.61 μC is much lower than the total stored charge of 50.16 μC (r = 53.05%). It indicates that a significant portion of original bound charges remains and a higher shock pressure is required to achieve complete depolarization. With further increasing the shock pressures from 4.5 to 6.6 GPa (Figs. S5c-d), the released current transforms into a quasi-square wave, and the value of Q increases from 35.72 to 46.82 μC with the r increasing from 71.21% to 93.34%, revealing that the ferroelectric ceramic is approaching complete depolarization (Fig. S5d). The amplitudes of currents and total released charges increase with increasing shock pressures.

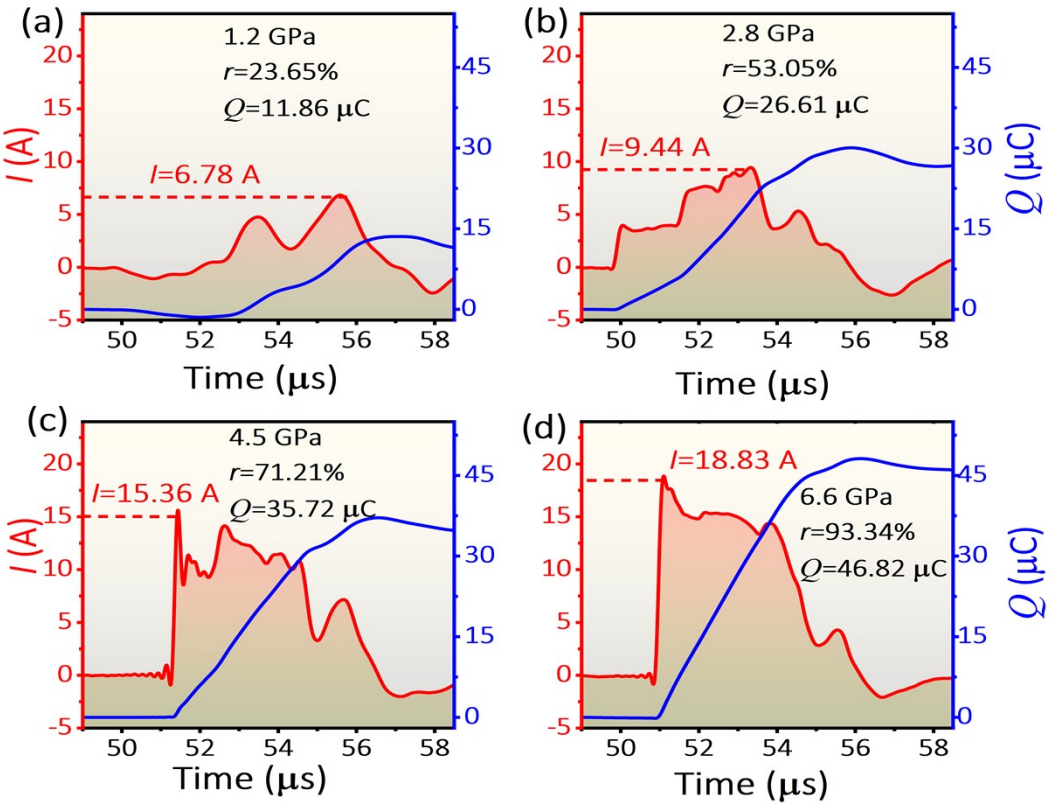

Fig. S5 Dynamic electric response of single-layer PMN-PZT+2Li films in the short-circuit mode under different shock pressures.

Fig. S6 shows the currents generated by the 34-layers ferroelectric film under different shock pressures. At low pressures (Figs. S6a-b), the current waveform characteristics are similar to those of the single-layer PMN-PZT+2Li films at low pressures (Fig. S5a). At this stage, the current is waving, presenting a pronounced piezoelectric effect. At 4.7 GPa, this multilayer film release 82.46% of the bound charges, and the peak current is 718 A (Fig. S6c). As increasing the pressure to 7.1 GPa, the multilayer film generates a peak current of 915 A with 1712.29 μC released, corresponding to 94.24% of the bound charges (Fig. S6d). Similar to the single-layer PMN-PZT+2Li film, the amplitudes of currents and total charges released by the 34-layer PMN-PZT+2Li film energy storage device increase with the increase of shock pressures.

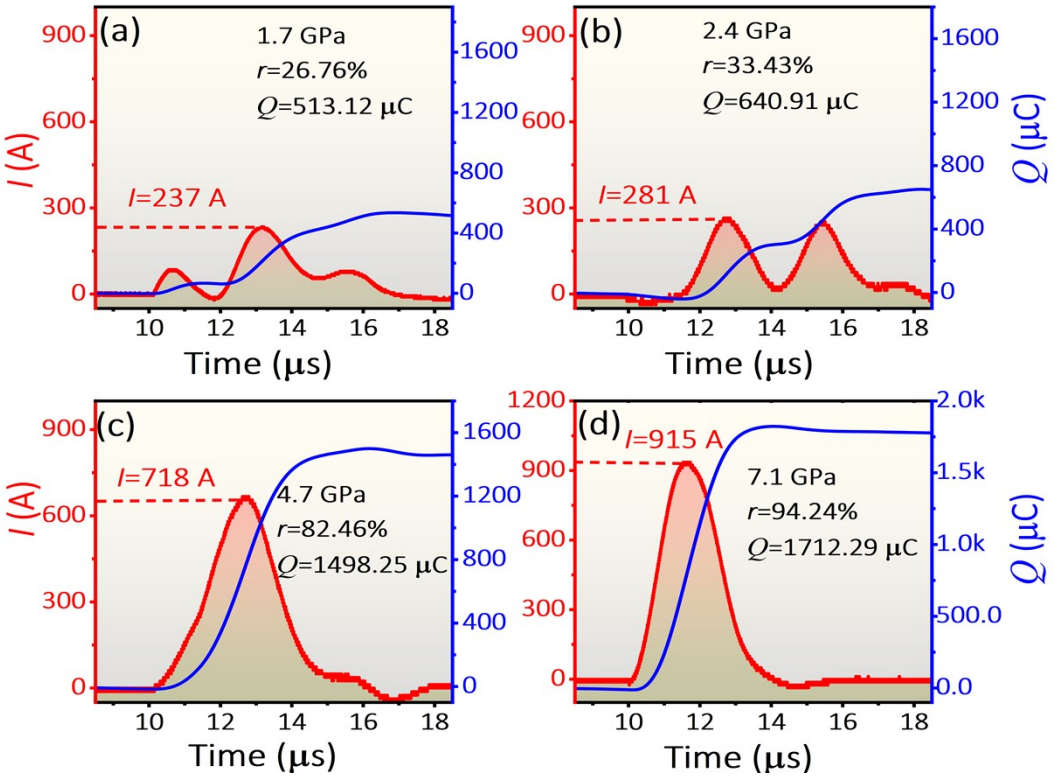

Fig. S6 Dynamic electric response of 34-layer PMN-PZT+2Li film energy storage devices in short-circuit mode under different shock pressures.

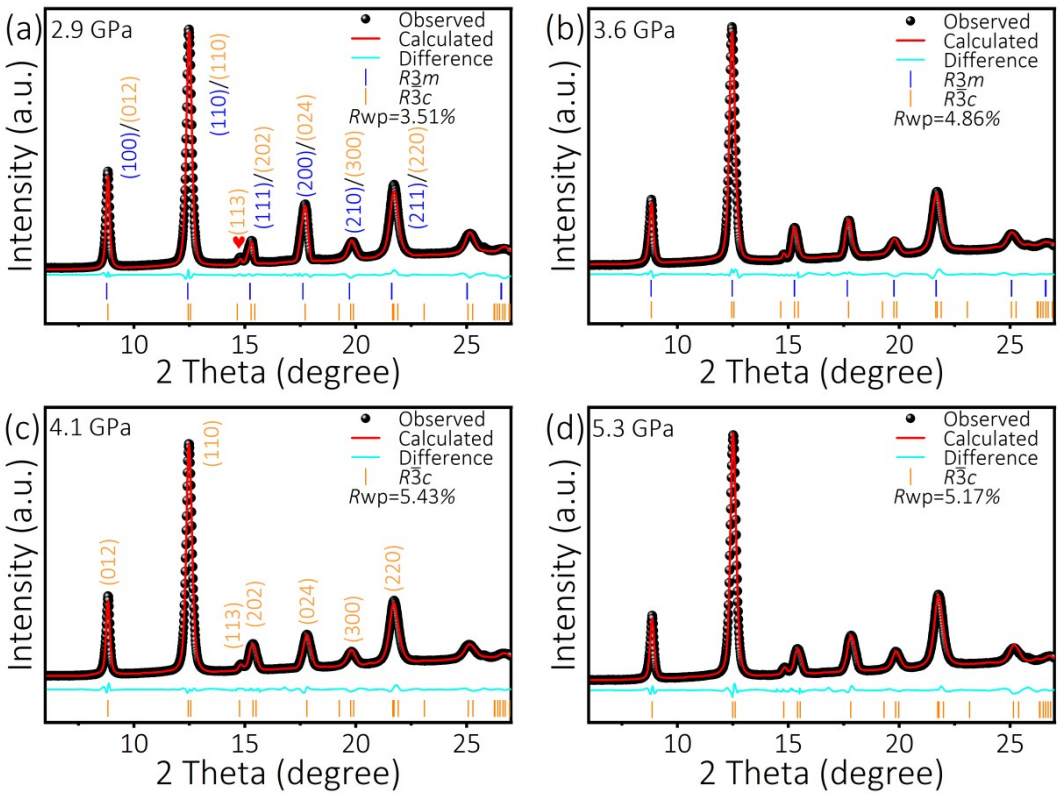

Fig. S7 Rietveld refinement of synchrotron X-ray diffraction data for PMN-PZT+2Li crystal under selected pressures.

Fig. S8 shows Rietveld refinement of XRD data of the PMN-PZT+2Li materials before (films) and after (powders) shock loading. Refinement results show that both the samples before and after loading possess a pure perovskite structure. The structural details are outlined in Table S3. Before loading, the unsplit {200} peak reveals that the PMN-PZT+2Li film sample is in a ferroelectric rhombohedral phase (Figs. S8a and S8b), corresponding to the [111] direction of the spontaneous polarization (Fig. 3e) [10, 11]. After loading, the splitting of the {200} reflection indicates a predominant tetragonal distortion (space group *P*4*mm*) with a [110] direction of spontaneous polarization (Fig. 3g) [10, 11]. However, a single-group refinement using *P*4*mm* shows poor fitting (Figs. S8c and S8d). Subsequently, combining *R*3*m* + *P*4*mm* phases provides a better fit to the diffraction patterns (Figs. S8e and S8f). The weight fractions of the *R*3*m* and *P*4*mm* phases are calculated to be 32.32% and 67.68%, respectively. It suggests that most of the PMN-PZT+2Li material transitions from the high-pressure phase back to the tetragonal phase rather than the rhombohedral phase after unloading. The differences observed in XRD measurements between the samples before and after loading suggest the high sensitivity of PMN-PZT+2Li to external mechanical processing. The complete depolarization of the PMN-PZT+2Li film cannot be explained by a shock-induced *R*3*m*→*P*4*mm* phase transition, unlike PZT 95/5 [12, 13], which is a polar-to-polar phase transformation. Moreover, *Shkuratov* et al. demonstrated through high-speed photographs that mechanical fragmentation of the PIN-PMN-PT single crystals was occurred after depolarization [14]. Therefore, the shock depolarization mechanism of

PMN-PZT+2Li films cannot be attributed solely to the pressure-induced phase transition from *R*3*m* to *P*4*mm*.

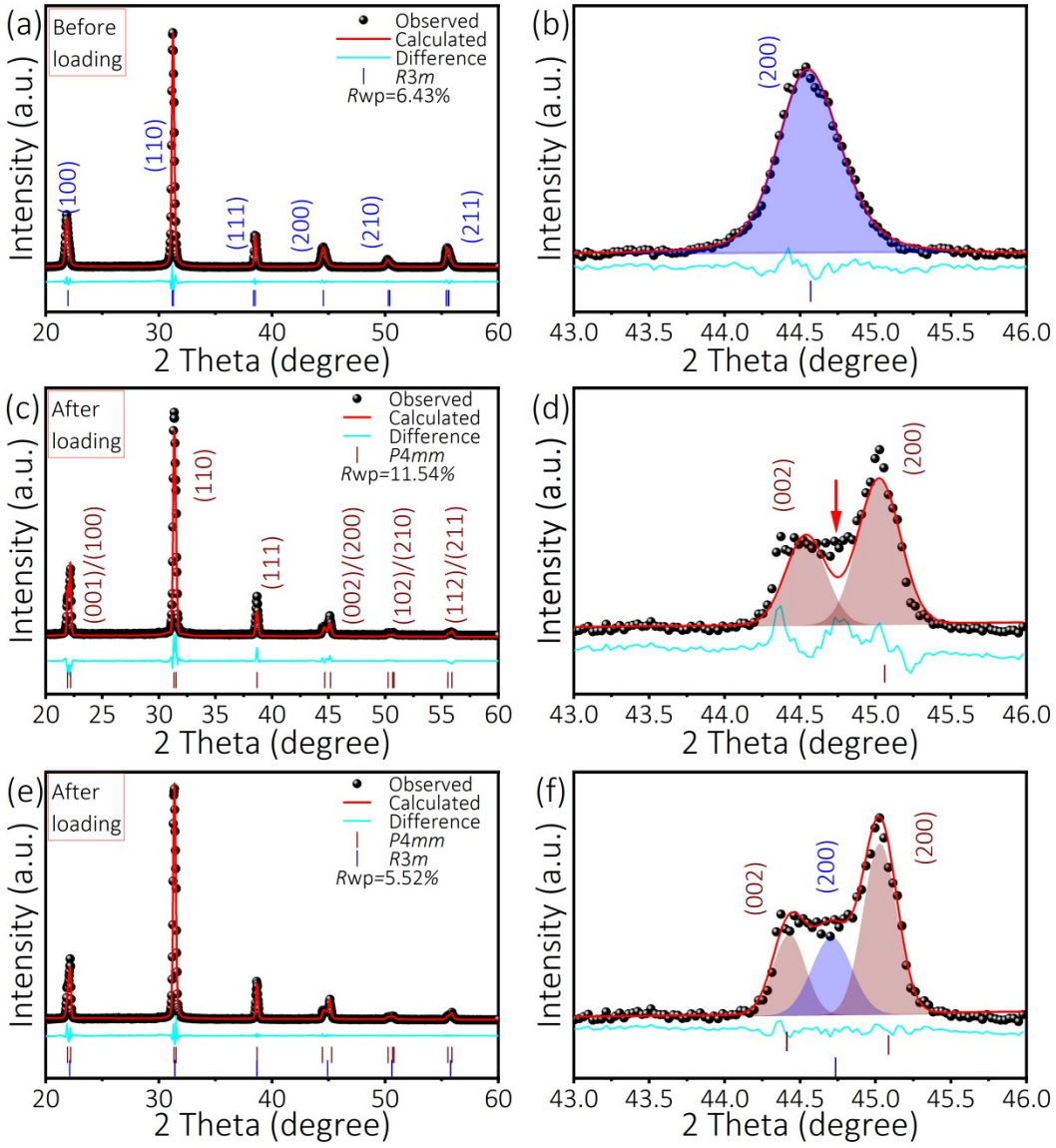

Fig. S8 (a,c,e) Rietveld refinement of X-ray diffraction data of PMN-PZT+2Li materials before and after loading, and (b,d, f) detailed variation of {200} peaks.

Fig. S9 illustrates the rhombohedral distortion (space group *R*3*m*) in the samples before and after polarization. When the film is broken into powders, a significant transformation occurs, mainly attributing to a tetragonal distortion (space group *P*4*mm*). The result is attributed to the transformation of films into powders, which inevitably results in residual stress and further compelling the movement of *B*-site atoms along the direction of spontaneous polarization [15].

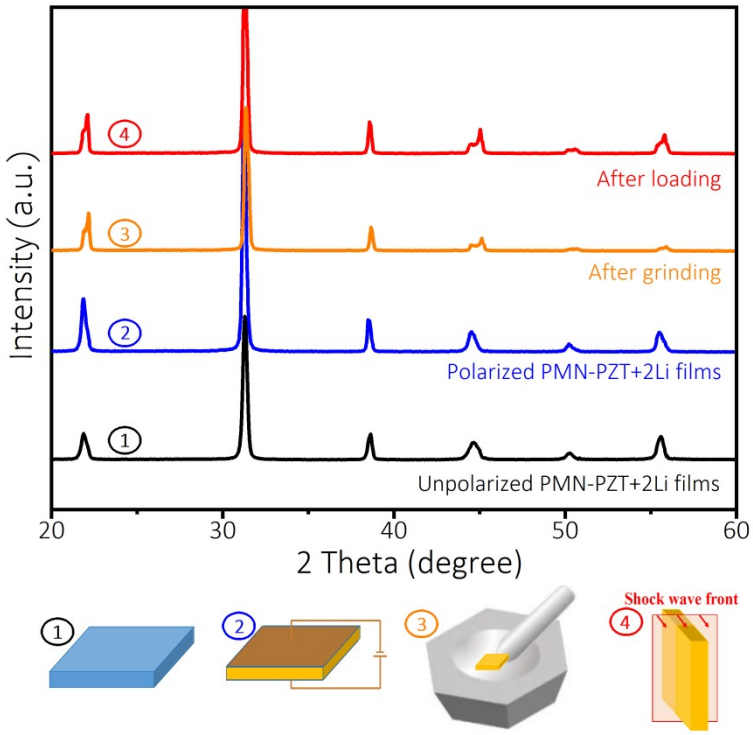

Fig. S9 XRD patterns of PMN-PZT+2Li materials in different states. ① Unpolarized films, ② film after electric polarization, ③ polarized film after grinding, ④ polarized film after shock loading.

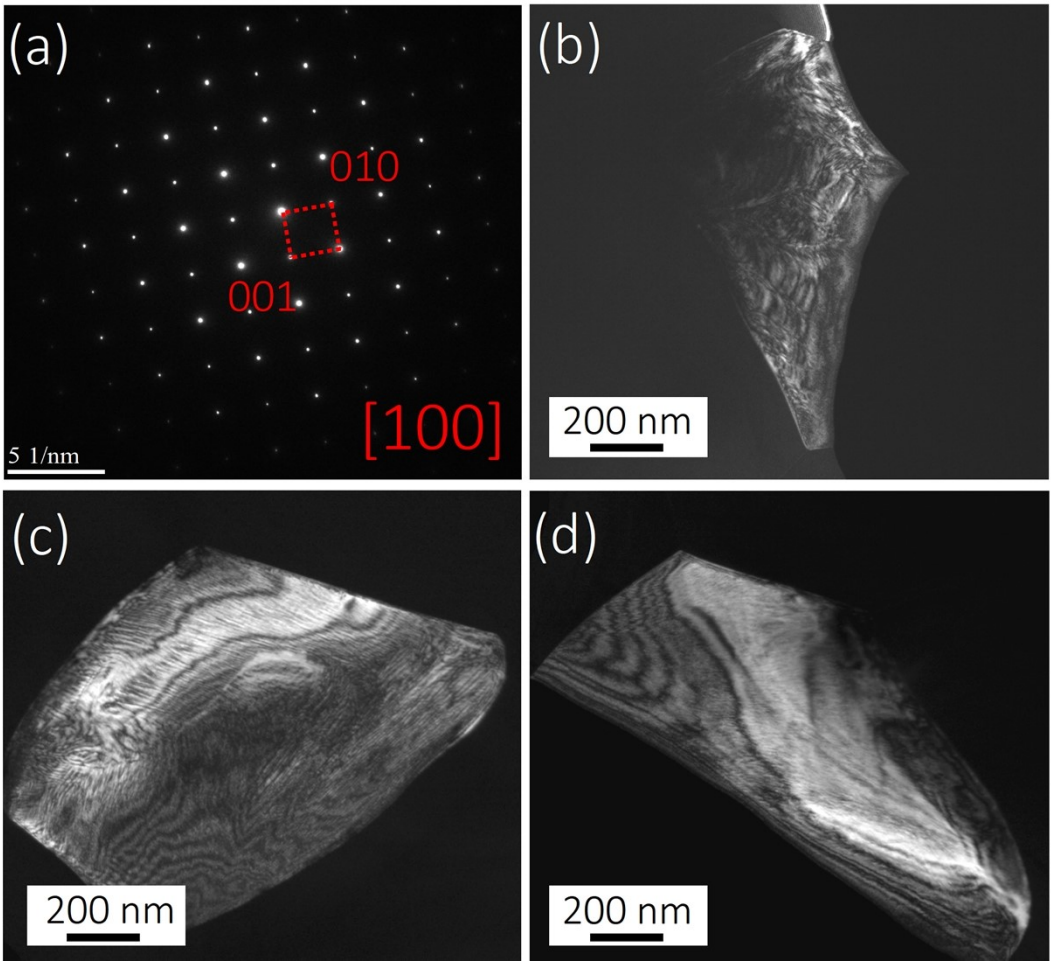

Fig. S10 The selected area electron diffraction pattern (a) and TEM scanning images (b-c) of PMN-PZT+2Li film.

Table S1 Refined atomic parameters for the PMN-PZT+2Li at room temperature and selected pressures.

Prsssure (GPa)		2.9		3.6		4.1	5.3
Space group		*R*3*m*	*Rc*	*R*3*m*	*Rc*	*Rc*	*Rc*
a (Å)		5.7211(6)	5.7174(5)	5.7194(6)	5.7109(2)	5.7084(5)	5.6923(7)
b (Å)		5.7211(6)	5.7174(5)	5.7194(6)	5.7109(2)	5.7084(5)	5.6923(7)
c (Å)		7.0245(7)	13.8651(3)	7.0101(5)	13.8193(9)	13.8088(7)	13.7586(6)
V(Å^3)		199.155(12)	392.518(11)	198.589(11)	390.329(14)	389.689(16)	386.084(14)
Z		3	6	3	6	6	6
α (degree)		90	90	90	90	90	90
β (degree)		90	90	90	90	90	90
γ (degree)		120	120	120	120	120	120
Pb	x	0	0	0	0	0	0
	y	0	0	0	0	0	0
	z	0	0.7503(8)	0	0.7501(7)	0.7497(5)	0.7501(5)
Mg/Nb/ Zr/Ti	x	0	0	0	0	0	0
	y	0	0	0	0	0	0
	z	0.4786(6)	0	0.4783(4)	0	0	0
O1	x	0.1581(5)	0.6633(5)	0.1582(6)	0.6083(4)	0.6085(8)	0.6096(6)
	y	-0.1581(5)	0.6633(5)	-0.1582(6)	0.6083(4)	0.6085(8)	0.6096(6)
	z	0.3483(2)	0.2503(7)	0.3482(5)	0.2502(6)	0.2504(7)	0.2503(8)
U_{ios} (Å^2)	Pb	1.017	0.872	0.865	1.032	1.023	0.476
	Mg/Nb /Zr/Ti	0.996	0.661	0.993	1.01	1.140	0.412
	O1	1.002	1.107	0.894	1.01	1.140	0.815
R_p (%)		3.49		4.37		5.21	4.74
R_{wp} (%)		3.51		4.86		5.43	5.17
ρ (g/cm^3)		8.112	8.230	8.134	8.276	8.290	8.367
fractions (%)		37.18	62.82	26.15	73.85	100	100

Table S2. Performance comparison of ferroelectric materials

	Released charge density /μC·cm^{-2}	Size (mm) wide×long× thick	Released charge /μC	Peak current /A	Peak current density /A·mm^{-3}	Output energy density /J·cm^{-3}	Depolarization temperature/°C	Ref.
$Pb(Zr_{0.95}Ti_{0.05})O_3$ (PZT 95/5) ceramics	32	5×5×5	8	6	0.048	0.068	50	[12]
	31.7	50.8×12.7× 12.7	204.5	20	0.002	/	50	[16]
	30	28×4×10	33.6	32	0.028	/	50	[1]
	32	30×20×2	192	40	0.013	/	50	[17]
	32.8	30×10×2	98.4	32	0.021	/	50	[18]
	34	30×10×2	102	40	0.027	/	50	[19]
	30.3	15×8×1	36.36	18.4	0.153	/	50	[20]
$Pb(Zr_{0.52}Ti_{0.48})O_3$ (PZT 52/48) ceramics	15	5×5×5	3.75	4	0.032	0.076	147	[12]
	14.3	50.8×12.7× 12.7	92.26	16	0.002	/	147	[16]
$Pb(In_{1/2}Nb_{1/2})O_3$-$Pb(Mg_{1/3}Nb_{2/3})O_3$-$PbTiO_3$ (PIN-PMN-PT) crystals	48	5×5×5	12	10	0.08	0.305	125	[12]
	32	5×5×5	8	7	0.056	/	125	[21]
	47	5×5×1	11.75	16	0.64	/	125	[14]
$Pb_{0.99}Nb_{0.02}[(Zr_{0.90}Sn_{0.10})_{0.96}Ti_{0.04}]_{0.98}O_3$ PZST ceramics	28.4	30×10×2	85.2	32	0.053	/	65	[18]
	27	25×4×3	27	32	0.16	/	65	[22]
	28	30×10×2	84	32	0.053	/	65	[19]
	28	30×10×2	84	30	0.05	/	65	[23]
$Bi_{0.5}Na_{0.5}TiO_3$-based ceramics	38	16×9×2	54.72	25	0.087	/	80	[24]
	38	16×8×2	48.64	26.4	0.103	0.147	80	[3]
	35	16×4×2	22.4	25	0.195	/	65	[25]
	28	11×7×1		15	0.195	/	140	[26]
$AgNbO_3$-based ceramics	38	16×8×2	48.64	22	0.086	/	155	[15]
$K_{0.5}Na_{0.5}NbO_3$ ceramics	17.5	8×4×2	5.6	6.6	0.103	0.293	188	[5]
Multilayer PZT 95/5 films	33.1	6.3×4.0×0.032 (120-layer)	1000.94	2297	3.281	3	50	[27]
Multilayer PMN-PZT films	32.56	12.5×12.5×0.045 (120-layer)	6105	3156	3.507	3.059	213	This work

Table S3 Refined atomic parameters for the PMN-PZT+2Li samples before and after shock loading

		Before loading	After loading	
Space group		*R*3*m*	*R*3*m*	*P*4*mm*
a (Å)		5.7234(9)	5.7145(9)	4.0295(6)
b (Å)		5.7234(9)	5.7145(9)	4.0295(6)
c (Å)		7.0397(8)	7.0036(5)	4.1001(9)
V(Å^3)		199.707(12)	198.073(18)	66.575(16)
Z		3	3	1
α (degree)		90	90	90
β (degree)		90	90	90
γ (degree)		120	120	90
Pb	x	0	0	0
	y	0	0	0
	z	0	0	0
Mg/Nb/Zr/Ti	x	0	0	0.5
	y	0	0	0.5
	z	0.4351(6)	0.4783(7)	0.4161(7)
O1	x	0.1580(5)	0.1581(7)	0.5
	y	-0.1582(6)	-0.1581(7)	0.5
	z	0.3484(7)	0.3482(6)	0.0491(7)
O2	x			0.5
	y			0
	z			0.5597(6)
U_{ios} (Å^2)	Pb	1.364	1.085	3.351
	Mg/Nb/Zr/Ti	0.865	0.293	0.332
	O1	1.119	0.916	1.723
	O2			1.225
R_p (%)		4.84	4.61	
R_{wp} (%)		6.43	5.52	
ρ (g/cm^3)		7.804	8.155	7.997
fractions (%)		100	32.32	67.68

Reference

[1] R. E. Setchell, J. Appl. Phys. 101 (2007) 053525.

[2] J. C. F. Millett, N. K. Bourne, D. Deas, J. Phys. D: Appl. Phys. 40 (2007) 2948-2953.

[3] Z. Gao, W. Peng, B. Chen, S. A. T. Redfern, K. Wang, B. Chu, Q. He, Y. Sun, X. Chen, H. Nie, W. Deng, L. Zhang, H. He, G. Wang, X. Dong, Phys. Rev. Mater. 3 (2019) 035401.

[4] Z. Zhou, Z. Gao, Z. Xiong, G. Liu, T. Zheng, Y. Shi, M. Xiao, J. Wu, L. Fang, T. Han, H. Liang,, H. He, Appl. Phys. Lett. 121 (2022) 113903.

[5] Z. Zhou, L. Fang, Z. Xiong, Y. Zhang, Y. Liu, G. Liu, Y. Liu, R. He, T. Han, J. Li, K. Wang, Z. Gao, Appl. Phys. Lett. 123 (2023) 012904.

[6] K. Xu, J. Li, X. Lv, J. Wu, X. Zhang, D. Xiao, J. Zhu, Adv. Mater. 38 (2016) 8519-8523.

[7] Q. Liu, Y. Zhang, J. Gao, Z. Zhou, H. Wang, K. Wang, X. Zhang, L. Li, J. Li, Energy Environ. Sci. 11 (2018) 3531.

[8] T. Sluka, A. K. Tagantsev, D. Damjanovic, M. Gureev, N. Setter, Nat. Commun. 3 (2012) 748.

[9] T. R. Shrout, S. Zhang, J. Electroceram 19 (2007) 111-124.

[10] K. Wen, J. Qiu, H. Ji, K. Zhu, J. Liu, J. Wang, J. Du, F. Zhu, J. Mater. Sci: Mater. El. 25 (2014) 3003-3009.

[11] X. Zhang, L. Yang, H. Ji, J. Qiu, J. Mater. Sci: Mater. El. 29 (2018) 3602-3610.

[12] S. I. Shkuratov, J. Baird, V. G. Antipov, E. F. Talantsev, J. Chase, W.

Hackenberger, J. Luo, H. R. Jo, C. S. Lynch, Sci. Rep. 7 (2017) 46758.

[13] S. Zhang, F. Li, X. Jiang, J. Kim, J. Luo, X. Geng, Prog. Mater. Sci. 68 (2015) 1-66.

[14] S. I. Shkuratov, J. Baird, V. G. Antipov, C. S. Lynch, S. Zhang, J. B. Chase, H. R. Jo, J. Mater. Chem. A 9 (2021) 12307.

[15] Z. Liu, T. Lu, F. Xue, H. Nie, R. Withers, A. Studer, F. Kremer, N. Narayanan, X. Dong, D. Yu, L. Chen, Y. Liu, G. Wang, Sci. Adv. 6 (2020) eaba0367.

[16] S. I. Shkuratov, J. Baird, V. G. Antipov, E. F. Talantsev, H. R. Jo, J. C. Valadez, C. S. Lynch, Appl. Phys. Lett. 104 (2014) 212901.

[17] G. Liu, F. Zhang, J. Du, H. Tan, H. He, Int. J. Mod. Phys. B 22 (2008) 1171-1176.

[18] D. Jiang, J. Du, Y. Gu, Y. Feng, J. Appl. Phys. 111 (2012) 024103.

[19] D. Jiang, J. Du, Y. Gu, Y. Feng, J. Appl. Phys. 111 (2012) 104102-10.

[20] H. Nie, Y. Yu, Y. Liu, H. He, G. Wang, X. Dong, J. Am. Ceram. Soc. 100 (2017) 5693-5699.

[21] S. I. Shkuratov, J. Baird, V. G. Antipov, W. Hackenberger, J. Luo, S. Zhang, C. S. Lynch, J. B. Chase, H. R. Jo, C. C. Roberts, Appl. Phys. Lett. 112 (2018) 122903.

[22] D. Jiang, N. Zhang, Y. Feng, J. Du, Y. Gu, Mater. Sci. Eng. B 177 (2012) 210-216.

[23] D. Jiang, J. Du, Y. Gu, Y. Feng, High Pressure Research 32 (2012) 280-290.

[24] P. Peng, H. Nie, G. Wang, Z. Liu, F. Cao, X. Dong, Appl. Phys. Lett. 113 (2018) 082901.

[25] Z. Xiong, G. Liu, H. Nie, Y. Liu, Z. Gao, Q. Liu, X. Chen, J. Li, L. Fang, Q. Yang, X. Zhang, J. Tang, G. Wang, X. Dong, J. Am. Ceram. Soc. 104 (2021) 1169-1177.

[26] Y. Liu, H. Nie, M. Xie, F. Cao, P. Peng, G. Wang, Appl. Phys. Lett. 123 (2023) 083903.

[27] S. I. Shkuratov, J. Baird, V. G. Antipov, S. Zhang, J. Chase, Adv. Mater. 31 (2019) 1904819.